Applied Catalysis B: Environmental 309 (2022) 121258

Contents lists available at ScienceDirect

Applied Catalysis B: Environmental

journal homepage: www.elsevier.com/locate/apcatb

Self-activated $Ni(OH)_2$ cathode for complete electrochemical reduction of trichloroethylene to ethane in low-conductivity groundwater

Jia Deng [a,b], Feng Wu [c], Shuxian Gao [d], Dionysios D. Dionysiou [e], Li-Zhi Huang [a,b,*]

[a] School of Civil Engineering, Wuhan University, No. 8, East Lake South Road, Wuhan, PR China
[b] State Key Laboratory of Water Resources and Hydropower Engineering Science, Wuhan University, 430072, PR China
[c] School of Resources and Environmental Science, Wuhan University, Wuhan, PR China
[d] CAS Key Laboratory of Urban Pollutant Conversion, Department of Applied Chemistry, University of Science and Technology of China, Hefei 230026, PR China
[e] Environmental Engineering and Science Program, Department of Chemical and Environmental Engineering, University of Cincinnati, Cincinnati, OH 45221-0012, United States

ARTICLE INFO

Keywords:
Hydrodechlorination
Trichloroethylene
Atomic hydrogen
Self-activated
Complete electrochemical reduction

ABSTRACT

This study investigates the electrochemical dechlorination of trichloroethylene (TCE) to non-toxic and value-added ethane by self-activated $Ni(OH)_2$ cathode. The $Ni(OH)_2$ cathode was fabricated by drop-casting the as-synthesized $Ni(OH)_2$ suspensions on a glassy carbon electrode. At −1.0 V applied potential, 94.6% of TCE is reduced after 5 h of electrolysis. TCE is efficiently transformed to ethane at a wide pH range in simulated groundwater environment with low-conductivity. The air-exposed $Ni(OH)_2$ cathode can still dechlorinate 49.8% TCE, showing the antioxidative capacity of $Ni(OH)_2$ cathode is superior than that of pristine Ni electrode. Both the directly transferred electrons and the generated atomic H* at the active Ni(0) sites contributed to the hydrodechlorination of TCE. Our work not only provides an effective way to completely detoxify chlorinated organic contaminants (COCs) under environment-relevant conditions, but also proves a concept that the chemical energy in COCs can be harvested during their electrochemical reduction processes.

1. Introduction

Complete electrochemical reduction of toxic micropollutants to non-toxic or even value-added compounds under environmentally relevant conditions is challenging [1]. Trichloroethylene (TCE) is one of the most widely detected pollutants in groundwater worldwide, and the presence of TCE in environment has raised global concerns due to its potential carcinogenicity and toxicity even in low concentrations [2–4]. Electrochemical reductive dechlorination is reported as an efficient technology for the detoxification of TCE in contaminated groundwater [5,6]. However, the direct electrochemical reductive dechlorination needs an extremely negative potential with a high energy consumption [7,8]. Also, toxic lesser-chlorinated by-products, such as *cis*-dichloroethylene (*cis*-DCE), *trans*-DCE, *1,1*-DCE and vinyl chloride (VC), are usually produced and released into the environment causing a secondary pollution during electrochemical reduction of TCE [9–11]. Complete electrochemical reduction of TCE to one non-chlorinated product could not only avoid secondary pollution but also favor the possible recovery and reuse of the as-formed dechlorination product [12]. Compared to wastes that have been intensively studied for their value-added conversion [13,14], micropollutants are more toxic and much widely distributed in the environment. Although the concentration of micropollutants such as TCE in the environment is usually deemed as low, the total amount is large due to the fact that hundreds of kilotons of TCE have been produced annually worldwide and 99% of them is emitted to the environment after use [15]. However, previous studies only focus on the electrochemical detoxification of TCE, and its complete electrochemical reduction to value-added products is largely ignored.

Comparing with direct electrochemical reduction, indirect reduction involving highly reactive atomic hydrogen (H*, $E^0 = -2.106$ V) shows excellent hydrodechlorination activity without the formation of toxic lesser-chlorinated by-products [16,17]. Transition metal electrocatalysts, especially Pd-based materials, could efficiently generate H* in water via catalytic reduction of H^+/H_2O [18–22]. H* can be generated on the surface of Pd electrode at potentials more negative than −0.65 V vs. Ag/AgCl [23,24]. The generated H* adsorbed on the surface of Pd can be used as reductant for COCs, or following Heyrovsky/Tafel steps to form H_2 [17,25,26]. However, large-scale application of Pd electrode is

* Corresponding author at: School of Civil Engineering, Wuhan University, No. 8, East Lake South Road, Wuhan, PR China.
E-mail address: lizhihuang@whu.edu.cn (L.-Z. Huang).

https://doi.org/10.1016/j.apcatb.2022.121258
Received 17 August 2021; Received in revised form 23 February 2022; Accepted 24 February 2022
Available online 26 February 2022

not feasible due to its high cost [27]. Ni shows a similar catalytic activity as Pd for H* generation but has a much lower price than Pd [28,29]. Nano zero-valent iron (n-ZVI) can reduce Ni^{2+} to Ni(0), which catalyzes the transformation of H^+/H_2O to H* for hydrodechlorination [30–32]. Ni-based electrocatalysts exhibit high electrocatalytic performance in HER where H* could form as an intermediate [33–35]. Ni content in stainless steel cathode highly influences the electrochemical hydrodechlorination of TCE [36]. However, pristine Ni electrode has a very low reactivity towards the electrochemical dechlorination of chlorinated organic contaminants (COCs). Ni has a relatively low oxidation potential (0.236 V), and a dense Ni oxide film easily forms on the surface of Ni electrode in oxic conditions. The passive Ni oxide film is reported to significantly weaken the electron transfer during the reduction process, which inhibits the Ni-mediated dechlorination of COCs [37].

$Ni(OH)_2$ is a promising electrocatalyst for HER due to its low cost, easy synthesis, stable structure, and high catalytic performance [38–41]. Also, it has been reported that $Ni(OH)_2$ could effectively split water molecules to produce H* [42,43]. $Ni(OH)_2$ is stable in an oxic environment. Also, porous $Ni(OH)_2$ thin-film structure could shorten ion diffusion paths and facilitate the rapid migration of electrolyte ions [44]. Ni(0) can be produced via the reduction of $Ni(OH)_2$. Ultrathin Ni (0)-embedded $Ni(OH)_2$ nanosheets (Ni(0)-$Ni(OH)_2$) formed by chemical reduction of $Ni(OH)_2$ shows superior HER activity due to the presence of Ni(0)-Ni(II) sites [45]. It is hypothesized that Ni(0) and $Ni(OH)_2$ may show a synergistic effect for H* generation. However, neither Ni $(OH)_2$ nor Ni(0)-$Ni(OH)_2$ has yet been used for the electrochemical hydrodechlorination of COCs in water.

In this work, Ni(0)-$Ni(OH)_2$ was formed via electrochemical reduction of $Ni(OH)_2$ and used for the hydrodechlorination of TCE to selectively produce ethane in low-conductivity groundwater. The structure and electrochemical property of Ni(0)-$Ni(OH)_2$ were characterized. The hydrodechlorination activity of self-activated $Ni(OH)_2$ cathode, influence of reaction parameters, and dechlorination mechanism were investigated both experimentally and theoretically.

2. Materials and methods

2.1. Chemicals and materials

Trichloroethylene (TCE), sodium sulfate (Na_2SO_4), sodium hydroxide (NaOH), nickel chloride hexahydrate ($NiCl_2{\cdot}6H_2O$), anhydrite calcium sulfate ($CaSO_4$), magnesium sulfate heptahydrate ($MgSO_4{\cdot}7H_2O$), ferrous sulfate ($FeSO_4$), humic acid, hydrochloric acid (HCl), and sulfuric acid (H_2SO_4) were purchased from Sinopharm Chemical Reagent Co. Ltd., China. Methanol was obtained from Sigma-Aldrich (Shanghai) Co. LLC., China. All reagents were analytical reagents and prepared using ultrapure water with a resistivity of 18.2 MΩ·cm. Glassy carbon electrodes (2 cm × 2 cm × 0.05 cm) were purchased from Shanghai Precision Scientific Instruments Co., Ltd. Nafion (D-520, polymer content (5%)) was obtained from Shanghai Branch, Du Pont China Holding Co., Ltd. The standard gasses of ethylene (C_2H_4) and ethane (C_2H_6) were purchased from Wuhan Zhongxinruiyuan Co., Ltd.

2.2. Characterization

$Ni(OH)_2$ particles were obtained by filtering and air-drying $Ni(OH)_2$ suspension. In order to collect the formed Ni(0)-$Ni(OH)_2$ particles, the self-activated $Ni(OH)_2$ cathode in electrochemical cell was moved into anoxic glovebox immediately after reaction followed by drying under inert conditions. X-ray diffraction (XRD, X′Pert PRO, PANalytical, Netherlands) was used to characterize the crystal structure of $Ni(OH)_2$ and the as-formed Ni(0)-$Ni(OH)_2$. X-ray photoelectron spectroscopy (XPS, ESCALAB250Xi, Thermo VG Scientific, USA) was used to determine the valence states and elemental composition of the materials. The morphological properties of the samples were analyzed by scanning electron microscopy (SEM) and transmission electron microscopy (TEM) characterization methods. The concentrations of dissolved Ni^{2+} in solution after electrolysis were determined by inductively coupled plasma-optical emission spectrometry (ICP-OES730, Agilent, USA).

2.3. Electrochemical reduction of TCE to ethane

The $Ni(OH)_2$ cathode was fabricated by drop-casting the as-synthesized $Ni(OH)_2$ suspensions on a glassy carbon electrode. Briefly, NaOH was slowly added into an aqueous solution containing 50 mM $NiCl_2$ until pH 8.0 to form $Ni(OH)_2$ precipitates (Fig. S1). After two hours of vigorous stirring, the $Ni(OH)_2$ suspensions were allowed to stand still for 24 h. Subsequently, 1.8 mL of $Ni(OH)_2$ suspensions and 0.2 mL of Nafion were mixed. The mixed solution (0.4 mL) was evenly smeared on both sides of a pre-polished glassy carbon electrode and air-dried. The Ni $(OH)_2$-coated glassy carbon electrode was used as the working electrode, a Pt plate as counter electrode, and a leak-free Ag/AgCl electrode as reference electrode. Electrochemical reduction of TCE and electrochemical analysis including cyclic voltammetry (CV), linear sweep voltammograms (LSV), electrochemical impedance spectroscopy (EIS) and open-circuit potentials (OCP) were conducted using an electrochemical workstation (CHI 600E, CH Instruments, USA). The reduction of TCE was carried out in a 50 mL electrochemical cell consisting of 30 mL 2 mM Na_2SO_4 solution and 20 mL headspace (Fig. S2). An aqueous solution consisting of 2 mM Na_2SO_4 was used as synthetic groundwater in this work, whose conductivity is similar to real groundwater [46]. The reaction solution was stirred for 30 min before electrochemical reaction to establish an equilibrium of TCE in solution and headspace. The analytical method of TCE and dechlorination products was detailed in text S1. In a control experiment, Ni electrode was used for TCE reduction and the preparation of Ni electrode was detailed in text S2. During stability investigation experiments, the electrode was moved into anoxic glovebox between each cycle experiment to protect the electrode from oxidation. Also, the electrochemical cell was filled with O_2-free electrolyte to protect the electrode from oxidation.

2.4. DFT calculations

The conformation of $Ni(OH)_2$ and Ni(0) cluster was optimized based on B3LYP [47,48] density functional theory (DFT) using Gaussian 09 package (Revision B.01) [49]. A mixed basis set including LANL2DZ for metal elements [50] and 6–311++G(d, p) for non-metallic elements [51] was selected. The solvation model based on density (SMD) implicit solvent was utilized throughout to mimic an aqueous environment [52]. The conformations of molecules with the highest occupied molecular orbital (HOMO) and lowest unoccupied molecular orbital (LUMO) were obtained by the Multiwfn [53]. The natural bond orbital (NBO) method was used to provide atomic charges [54].

3. Results and discussion

3.1. Self-activation of $Ni(OH)_2$ during TCE reduction

Pristine Ni electrode was used for TCE electrochemical reduction and the XRD patterns of the pristine Ni electrode was shown in Fig. S3a. A part of TCE (35.6%) was dechlorinated to C_2H_4 (12.6%) and C_2H_6 (21.1%) after 5 h of electrolysis at −1.0 V (Fig. S3b), demonstrating the hydrodechlorination reactivity of the un-passivated Ni electrode. However, the electrochemical dechlorination performance of the Ni electrode was diminished completely after exposing in air for 24 h (Fig. S3c). After being polished under anaerobic conditions, the dechlorination activity of the oxidized Ni electrode was partially restored (Fig. S3d). The current density for the air-exposed Ni electrode decreased compared with that for the pristine Ni electrode, and the current density increased after electrode polishing (Fig. S3e). These results demonstrated that electron transfer from the cathode to TCE was hindered by the dense oxide layer formed on the surface of Ni electrode (Fig. S3f) [55].

CV of $Ni(OH)_2$ suspension shows a reduction peak at approximately −0.8 V during the cathodic scan (Fig. 1a), indicating Ni(II) is reduced to Ni(0) when the potential was more negative than −0.8 V (Eq. 1) [56]. Thus, the $Ni(OH)_2$-coated glassy carbon cathode might be self-activated to form Ni(0)-$Ni(OH)_2$ cathode at −1.0 V. As shown in Fig. 1b, the self-activated $Ni(OH)_2$ cathode showed excellent performance for TCE reduction with the TCE removal efficiency reaching 94.6% after 5 h of electrolysis. TCE was almost completely transformed to C_2H_6. No toxic lesser-chlorinated intermediates such as DCE and VC were detected during the electrochemical reduction process (Fig. S4), demonstrating a highly efficient hydrodechlorination process of TCE to C_2H_6. In contrast, TCE removal was negligible in the presence of Ni^{2+}/$Ni(OH)_2$ (Fig. S5a). TCE cannot be efficiently dechlorinated by bare glassy carbon electrode, because the dechlorination potential of TCE was more negative than −1.0 V (Fig. S5b) [6]. Thus, the self-activation process of $Ni(OH)_2$ with the formation of Ni(0)-$Ni(OH)_2$ may play an important role in the hydrodechlorination of TCE and the active sites were further identified in the following experiments.

$$Ni(II) + 2e^- \rightarrow Ni(0) \quad (1)$$

$Ni(OH)_2$ particles were collected for characterization before reaction. XRD patterns confirmed that the as-synthesized $Ni(OH)_2$ was β-$Ni(OH)_2$, which was isostructural as brucite (Fig. 1c) [57]. The particles deposited on the electrode were characterized after the electrochemical reaction. Although the diffraction peaks derived from the glassy carbon electrode are intense (Fig. S6), the diffraction peak of β-$Ni(OH)_2$ is evident (Fig. 1d). Also, the diffraction peaks at 51.2° and 75.4° correspond to the (200) and (220) planes of Ni(0), respectively. Ni 2p XPS of $Ni(OH)_2$ shows a peak at 855.7 eV corresponding to the Ni^{2+} in $Ni(OH)_2$ and the peak at 852.3 eV corresponding to Ni(0) was detected after reaction (Fig. 1e) [45]. The contents of Ni(0) and Ni(II) were 0% and 100% before the reaction which change to 10.2% and 89.8% after reaction. In addition, three O species including lattice O in metal oxides at 531.4 eV, hydroxide O (Ni−O−H) at 532.7 eV, and chemisorbed O at 535.1 eV were determined in O 1s XPS of $Ni(OH)_2$ (Fig. 1f) [58]. After the reaction, chemisorbed O disappeared and hydroxide O decreased confirming the reduction from Ni(II) to Ni(0) because of the dehydroxylation of Ni$(OH)_2$. SEM images show β-$Ni(OH)_2$ has an irregular platy morphology (Fig. S7a) and the particles after reaction retain the platy morphology (Fig. S7b). HRTEM images show a lattice spacing of 4.8 Å corresponding to the (001) plane of $Ni(OH)_2$ (Fig. 1g). Also, lattices with a spacing of 1.2 Å stem from the (220) plane of Ni(0) (Fig. 1h). A part of Ni(II) was electrochemically reduced to Ni(0) in $Ni(OH)_2$ leading to the formation of the Ni(0)-$Ni(OH)_2$ composite. As a result, $Ni(OH)_2$ cathode was self-activated electrochemically.

3.2. Electrochemical characterization

The LSV of Ni, glassy carbon, $Ni(OH)_2$ and Ni(0)-$Ni(OH)_2$ electrodes were compared (Fig. 2a). When the potential was more negative than −0.8 V, the cathodic current density of Ni(0)-$Ni(OH)_2$ was larger than those of the other electrodes. The large cathodic current density indicates Ni(0)-$Ni(OH)_2$ has the highest catalytic activity for water reduction among the studied electrodes, which may be associated with the high reactivity for H* generation. Comparing with the $Ni(OH)_2$, the Ni(0)-$Ni(OH)_2$ shows a smaller arc radius in EIS indicating Ni(0)-Ni$(OH)_2$ has a faster interfacial charge transfer rate than $Ni(OH)_2$ (Fig. 2b). The OCP of $Ni(OH)_2$ was positive, because $Ni(OH)_2$ cannot be oxidized in water (Fig. 2c). In contrast, the OCP of Ni(0)-$Ni(OH)_2$ was negative proving electrons were transferred from Ni(0)-$Ni(OH)_2$ to bulk solution. The non-faradaic capacitive current can be calculated by running a series of CVs at different scan rates around the OCP (text S3, Fig. S8) [59]. The capacitance of Ni(0)-$Ni(OH)_2$ electrode was 1.94 mF which was higher than 1.41 mF of $Ni(OH)_2$ electrode (Fig. 2d). Since the capacitive current is proportional to electrochemically active surface area (EASA) [60], the EASA of Ni(0)-$Ni(OH)_2$ electrode (48.50 cm^2) was higher than that of $Ni(OH)_2$ electrode (35.25 cm^2). In brief, the electron donating ability and EASA were both increased during self-activation process of $Ni(OH)_2$ cathode, which was essential for electrochemical reduction from TCE to ethane.

3.3. Effect of potential

In order to further investigate the effect of Ni(0) on the electrochemical reduction of TCE to ethane, electrolysis was conducted under different potentials. Only 10.8% of TCE was removed at −0.5 V after 5 h of electrolysis and no dechlorination products were observed (Fig. 3a). In addition, Cl^- was not detected in reaction solution at −0.5 V (Fig. S9a) indicating $Ni(OH)_2$ cathode cannot efficiently reduce TCE in the absence of Ni(0). The 10.8% TCE removal may be attributed to the electrostatic adsorption between TCE and $Ni(OH)_2$ at −0.5 V [61]. When the potential was −0.8 V, the removal efficiency of TCE reached 44.4% after 5 h. A trace amount of dechlorinated product was formed (Fig. 3b) and Cl^- with a low concentration was detected in solution (Fig. S9b), indicating the $Ni(OH)_2$ was self-activated at −0.8 V and initiated the dechlorination. Since the reduction peak from Ni(II) to Ni(0) was at −0.88 V (Fig. 1a), the amount of produced Ni(0) could be small at −0.8 V. The low content of Ni(0) in Ni(0)-$Ni(OH)_2$ composite led to a low reduction efficiency of TCE. When the applied potential decreased from −0.8 V to −0.9 V, 93.3% of TCE was removed after 5 h and 36.5% of TCE was transformed to C_2H_6 (Fig. 3c). The change in chlorine balance curve was consistent with the change in carbon balance curve (Fig. S9c). When the applied potential was more negative than −1.0 V, almost all of the TCE was reduced to C_2H_6 (Figs. 1b and 3d), demonstrating the complete self-activation of $Ni(OH)_2$ was beneficial to the hydrodechlorination of TCE. The concentration changes of Cl^- at −1.0 V and −2.0 V were close (Fig. S9d–e), which conformed with the result of TCE reduction. The change of current densities for TCE hydrodechlorination under different potentials is shown in Fig. S10. When the applied potential decreased from −0.8 V to −1.0 V where reduction from Ni(II) to Ni(0) occurs, the current density increases with time proving that self-activated Ni(0) accelerates the electron transfer from the cathode to TCE molecules. Furthermore, the growth rate of current density increased with the potential decreasing from −0.8 V to −1.0 V, reflecting the $Ni(OH)_2$ cathode had a higher self-activated rate at −1.0 V than at −0.9 V and −0.8 V. TCE reduction efficiency was similar at −1.0 V and −2.0 V, indicating the performance of Ni(0)-$Ni(OH)_2$ for TCE reduction was level-off when the applied potential was more negative than −1.0 V. Although the current density of −2.0 V potential was higher than −1.0 V, the slopes of curves were similar, indicating the potentials more negative than −1.0 V may not further enhance the production of Ni(0) but only favor HER. Fig. S11 showed the on-set potential of HER was higher for $Ni(OH)_2$ self-activated at −2.0 V than that at −1.0 V, indicating $Ni(OH)_2$ self-activated at −2.0 V had a higher HER activity. However, the self-activated $Ni(OH)_2$ cathode at −2.0 V had higher normalized energy consumption (*EC*) value (text S4) than that at −1.0 V due to the strong HER (Fig. S12). Thus, the self-activated $Ni(OH)_2$ cathode at −1.0 V is more advantageous for application than that at −2.0 V.

Notably, an obvious carbon and chlorine mass loss was observed for the electrolysis at −0.8 V and −0.9 V. In order to find the reason of mass loss during electrolysis, we used concentrated hydrochloric acid to completely deconstruct the $Ni(OH)_2$ and the formed Ni(0)-$Ni(OH)_2$ on glassy carbon electrode (Text S5). Fig. S13a showed that a part of TCE was released after the deconstruction of $Ni(OH)_2$ on cathode with −0.8 V self-activation. In addition, TCE together with trace concentrations of *cis*-DCE and *1,2*-dichloroethane adsorbed on the electrode was released into headspace after acid digestion (Fig. S13b). Similarly, a part of TCE was released from the cathode after the deconstruction of Ni$(OH)_2$ self-activated at −0.9 V (Fig. S14a), and trace amounts of *1,1*-DCE and *cis*-DCE were also released (Fig. S14b). The rise of carbon balance

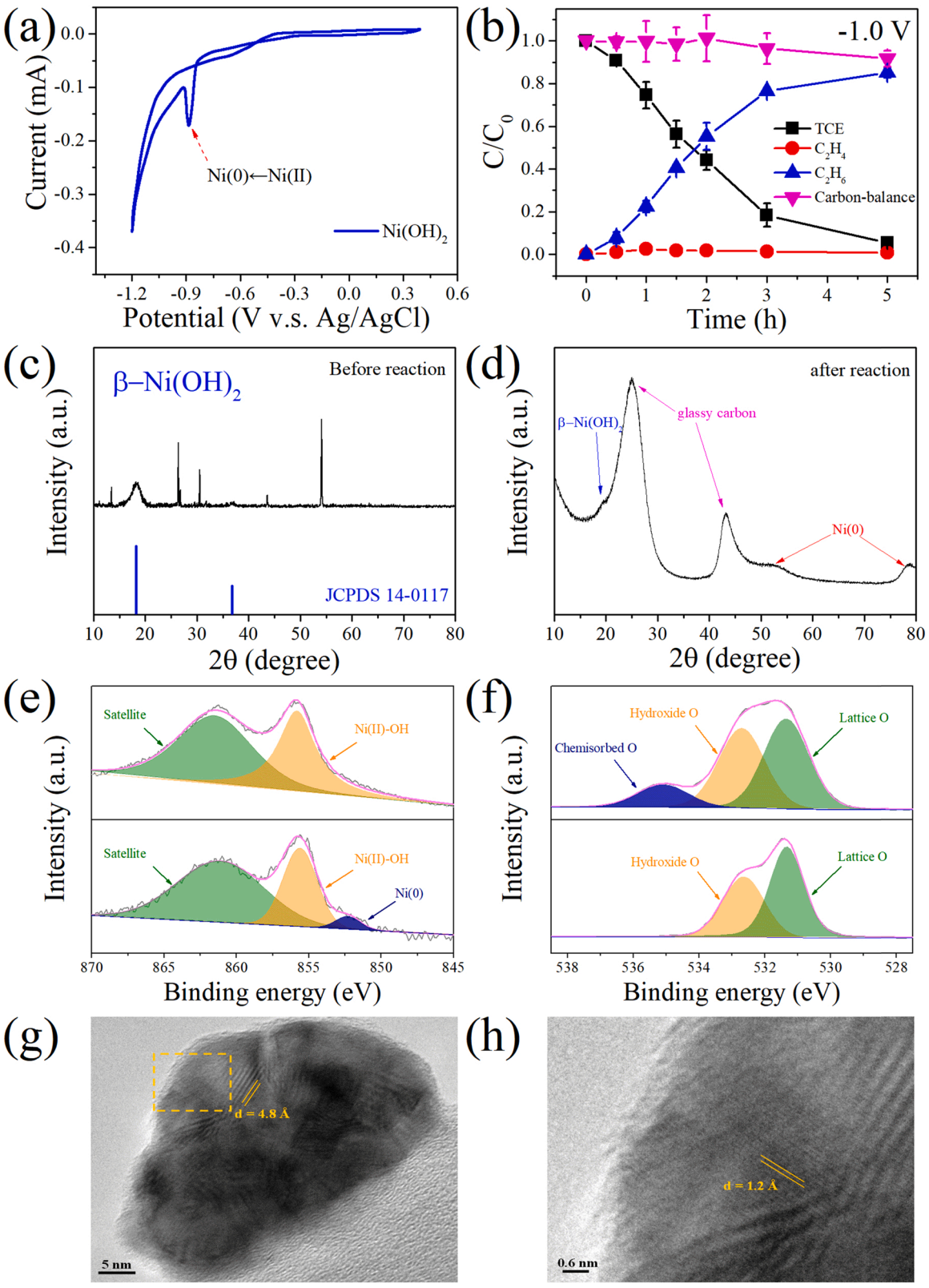

Fig. 1. (a) The CV of $Ni(OH)_2$ suspensions. Experimental conditions: pH = 7.0, electrolyte = 50 mM Na_2SO_4, glassy carbon working electrode. (b) Electrochemical reduction of TCE to ethane at −1.0 V in synthetic groundwater (2 mM Na_2SO_4 aqueous solution). Experimental conditions: pH = 7.0, initial TCE concentration = 25 μM. (c) XRD patterns of $Ni(OH)_2$ before reaction. (The other peaks are assigned to NaCl, JCPDS 05-0628). (d) XRD patterns of $Ni(OH)_2$ after reaction. (e) Ni 2p XPS of the particles on the electrode surface after reaction. (f) O 1s XPS before and after reaction. (g–h) High-resolution TEM images of Ni(0)-$Ni(OH)_2$.

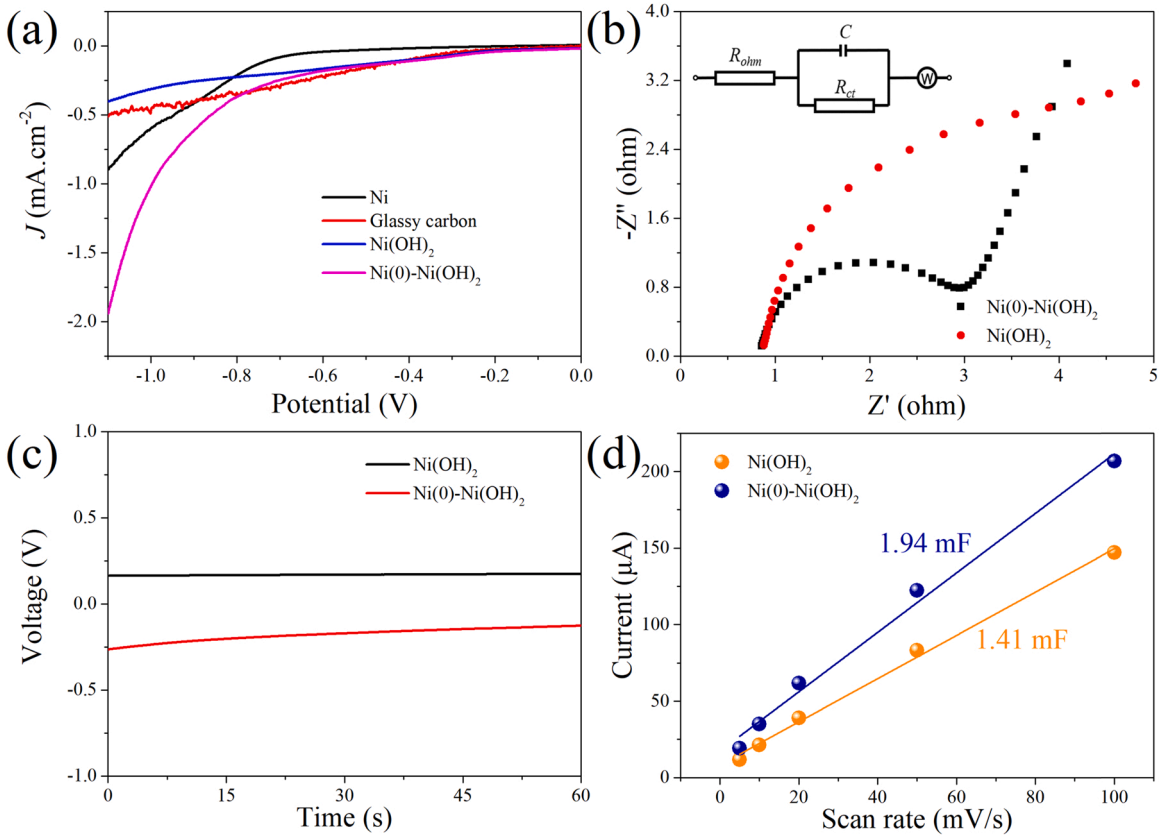

Fig. 2. (a) LSV of Ni, glassy carbon, $Ni(OH)_2$ and Ni(0)-$Ni(OH)_2$ cathode. (b) The Nyquist plots of $Ni(OH)_2$ and Ni(0)-$Ni(OH)_2$ cathode. (c) OCP of $Ni(OH)_2$ and Ni(0)-$Ni(OH)_2$ electrode vs. time. (d) Plots of current vs. scan rates of $Ni(OH)_2$ and Ni(0)-$Ni(OH)_2$ electrodes measured around the OCP vs. Ag/AgCl. Experimental conditions: temperature = 25 °C, electrolyte = 50 mM Na_2SO_4, frequency range = 0.01 Hz–100 kHz, pH = 7.0.

curves after acid digestion demonstrated that the adsorption of TCE and its dechlorination intermediates on the cathode was the main reason causing the carbon mass loss.

The electron selectivity efficiency (*ES*) at different applied potentials was investigated. As shown in Fig. 4a, the input electrons were consumed by Ni(II) reduction (e_r), TCE hydrodechlorination (e_d) and HER (e_H). The dissociation of one C-Cl bond needs two electrons [62,63]. Thus, the value of e_d can be calculated according to Eqs. 2–4. $C(Cl^-)$ represents the concentration of Cl^- in solution. The reaction solution volume is 0.03 L and N_A is Avogadro constant (6.02×10^{23}). The total electron input at different potentials is shown in Fig. 4b, and the total input electron number (e_0) can be calculated (1 C = 6.24×10^{18} e^-). The *ES* can be obtained from e_d/e_0. As shown in Fig. 4c, the *ES* value was extremely low when the potential was more positive than −0.8 V due to the inefficient reduction of Ni(II) to Ni(0). The *ES* value increased significantly when the potential decreased from −0.8 V to −1.0 V, indicating the e_d increased much faster than e_0 when the potential became more negative in this range. The HER dominated at −2.0 V which led to a decrease of *ES* value for TCE-to-ethane conversion. The highest *ES* value of −0.9 V and −1.0 V appeared at 0.5 and 1.0 h, respectively. At the initial reaction stage, the input electrons were mainly consumed as e_r due to the reduction of Ni(II) to Ni(0). The e_d decreased gradually with the transformation from TCE to ethane, which is attributed to the decreased concentration of TCE.

$$C_2HCl_3 + 3\ H^+ + 6e^- \rightarrow C_2H_4 + 3Cl^- \quad (2)$$

$$C_2HCl_3 + 5\ H^+ + 8e^- \rightarrow C_2H_6 + 3Cl^- \quad (3)$$

$$e_d = [C(Cl^-) \times 2] \times 0.03 \times N_A \quad (4)$$

3.4. Mechanism

The CVs of $Ni(OH)_2$ cathode and the Ni(0)-$Ni(OH)_2$ cathode were analyzed in order to identify the active species. Firstly, no obvious redox peaks of possible active species were observed in the CVs of $Ni(OH)_2$ cathode (Fig. S15). In contrast, three oxidation peaks in the range from −0.6 to −0.5, from −0.25 to −0.15, and from 0.15 to 0.30 V (vs. Ag/AgCl) were observed in CVs of Ni(0)-$Ni(OH)_2$ cathode which corresponded to the oxidation of H_2, H_{abs}* and H_{ads}* , respectively (Fig. 5a) [58,64]. In addition, one reduction peak at −0.3 V was also observed. This reduction peak and H_{abs}* oxidation peak appeared together when the potential was more negative than −0.3 V and disappeared together when the potential was less negative than −0.3 V (Fig. S16). Thus, the reduction peak at −0.3 V belongs to H_{abs}* . In the presence of 0.4 mM TCE, the oxidation peaks of H_{ads}* was not present demonstrating that H_{ads}* can react with TCE (Fig. 5b) [23]. Methanol as the quencher of H* (Eq. 5) was introduced into the electrolyte [65]. The oxidation peaks of H_{abs}* and H_{ads}* became less intense after the addition of methanol (Fig. 5c), confirming the quenching effect on H* . Furthermore, the oxidation peak of H_2 was also disappeared. Hydrogen evolution reaction (HER) occurred on the surface of zero-valent metal involving Volmer reaction and Tafel/Heyrovsky reaction (Eqs. 6–8) [30]. The oxidation peak of H_2 can be detected in CVs of the formed Ni(0)-$Ni(OH)_2$, because a part of H_2 remained in the vicinity of Ni(0) due to slow diffusion into bulk solution (Fig. S17) [66]. For the quenching experiment, although the added methanol in the electrolyte reacts with H* to generate H_2, the formed H_2 immediately leaves the electrode-solution interface and released into the bulk solution and headspace (Fig. S17), thereby causing the disappearance of the H_2 oxidation peak in CVs.

$$CH_3OH + H^* \rightarrow CH_2OH^* + H_2 \quad (5)$$

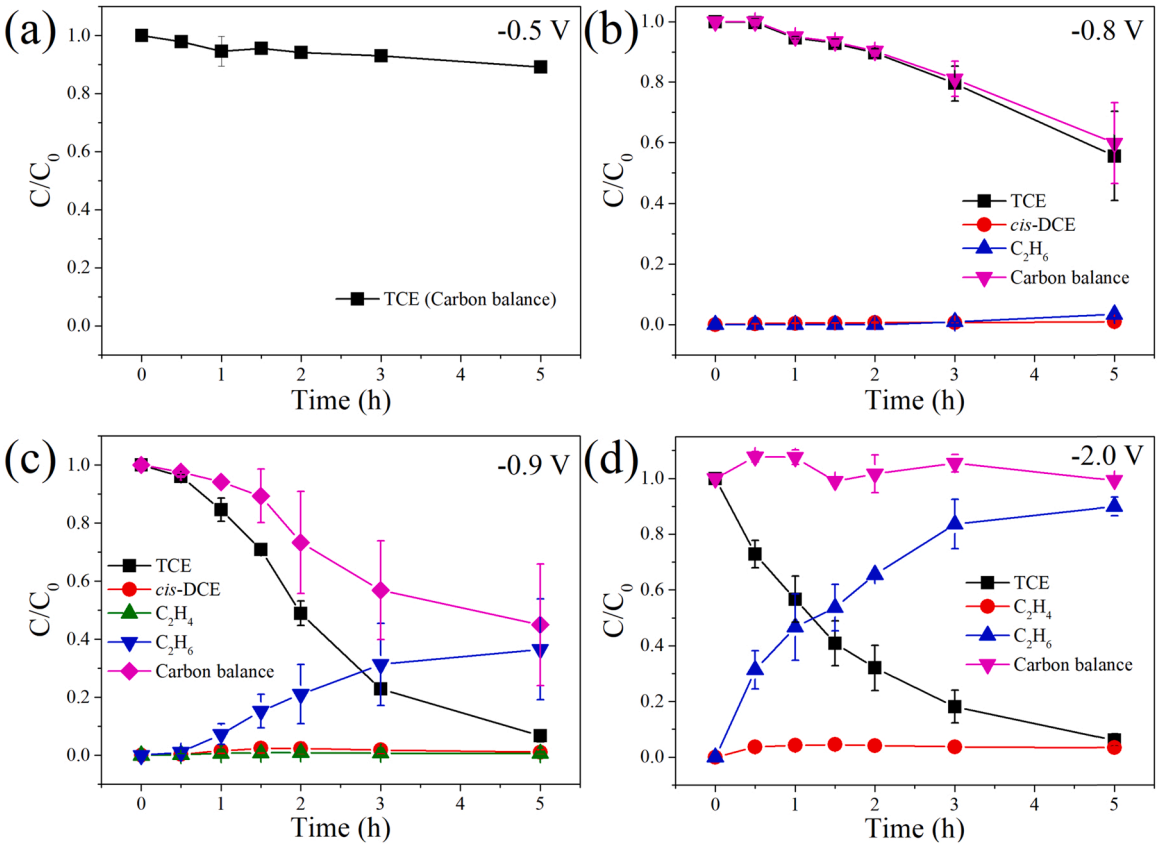

Fig. 3. Change of TCE, dechlorination products and carbon balance during electrolysis at (a) −0.5 V, (b) −0.8 V, (c) −0.9 V and (d) −2.0 V. Experimental conditions: electrolyte = 2 mM Na_2SO_4, initial TCE concentration = 25 μM, pH = 7.0.

$$H^+ + e^- + Ni(0) \rightarrow Ni(0)\text{-}H_{ads}* \quad (6)$$

$$Ni(0)\text{-}H_{ads}* + Ni(0)\text{-}H_{ads}* \rightarrow 2Ni(0) + H_2 \quad (7)$$

$$Ni(0)\text{-}H_{ads}* + H^+ + e^- \rightarrow Ni(0) + H_2 \quad (8)$$

$$C_2H_4 + 2H* \rightarrow C_2H_6 \quad (9)$$

Methanol was introduced into the electrochemical reduction process to investigate the role of H* . In the presence of 120 mM methanol, the production of C_2H_4 increased and the production of C_2H_6 decreased comparing with that without methanol (Fig. S18a). Since H* is responsible for the hydrogenation of C_2H_4 to C_2H_6 (Eq. 9), it is concluded that 120 mM of methanol can inhibit the conversion of C_2H_4 to C_2H_6. In order to exclude the influence of solvent effect, excess concentration of NO_3^- (120 mM) was added into the electrochemical system to induce competition of H* with TCE, because NO_3^- can be reduced to NO_2^- and NH_4^+ by H* [58]. As shown in Fig. S18b, 14.1% C_2H_4 and 77.9% C_2H_6 were generated in the presence of 120 mM NO_3^-. Meanwhile, 5.28 mM and 0.48 mM of NH_4^+ and NO_2^-, respectively, were formed. Notably, whether in the presence of 120 mM methanol or 120 mM NO_3^-, the removal and dechlorination efficiency of TCE was hardly affected. This result demonstrated that the presence of 120 mM methanol and NO_3^- did not affect the self-activation of $Ni(OH)_2$. In addition, TCE dechlorination was not only dependent on the H* , but it can also be attributed to direct electron transfer between Ni(0) sites with TCE.

Subsequently, we increased the concentration of methanol to 240 mM and 360 mM, and we found that the removal and dechlorination efficiency of TCE decreased dramatically (Fig. S19a–b). Specifically, the final complete dechlorination products contents were only 40.4% (3.0% C_2H_4 and 37.4% C_2H_6) in the presence of 240 mM methanol, and 22.7% (3.2% C_2H_4 and 19.5% C_2H_6) in the presence of 360 mM methanol (Fig. 5d). The calculated e_d values also decreased gradually with the increase of methanol concentration (Fig. 5e), demonstrating the electrons transfer between TCE and cathode was obviously inhibited. However, if 360 mM methanol was introduced into the electrolyte after one hour of electrolysis, the conversion from C_2H_4 to C_2H_6 was inhibited immediately whereas the removal and dechlorination of TCE was unaffected (Fig. 5f). This result indicates that the electron transfer process will not be hindered by methanol once Ni(0) sites are formed on $Ni(OH)_2$ cathode after one hour of electrolysis. As shown in Fig. S20, the self-activated $Ni(OH)_2$ cathode in the presence of 360 mM methanol after one hour of electrolysis had a similar HER activity as that without methanol. However, the self-activated $Ni(OH)_2$ cathode when 360 mM methanol was initially added had a relatively weak HER activity. This result demonstrated that the initial addition of 360 mM methanol inhibited the formation Ni(0), thereby inhibiting the reduction of TCE.

The $Ni(OH)_2$ cathode may be self-activated in two ways. The first way is that $Ni(OH)_2$ on cathode directly obtains the electrons to form Ni (0) sites (Fig. S21a). Notably, $Ni(OH)_2$ cathode had no obvious reduction peak at approximately −0.8 V (Fig. S15), which was different with the CVs result of $Ni(OH)_2$ suspensions (Fig. 1a). This result was attributed to the different electron transfer pathway. For $Ni(OH)_2$ suspensions, electrons from glassy carbon transfer to $Ni(OH)_2$ particles in electrode-solution interface for the reduction of $Ni(OH)_2$ (Fig. S21b). The formed Ni(0) sites catalyze H_2O/H^+ to generate H* . H* as a strong reductive species can further reduce Ni(II) to Ni(0), which is the second self-activation way. As shown in Fig. S22, the presence of methanol did not affect the reduction potential of $Ni(OH)_2$, indicating methanol did not affect the first pathway. Thus, the initial addition of 360 mM methanol affects the generation of Ni(0) sites through the second pathway. As shown in Fig. S23, the charging capacitance at ~0 V was significantly decreased with the increase in methanol concentration from 120 mM to 360 mM, indicating the added methanol was likely to

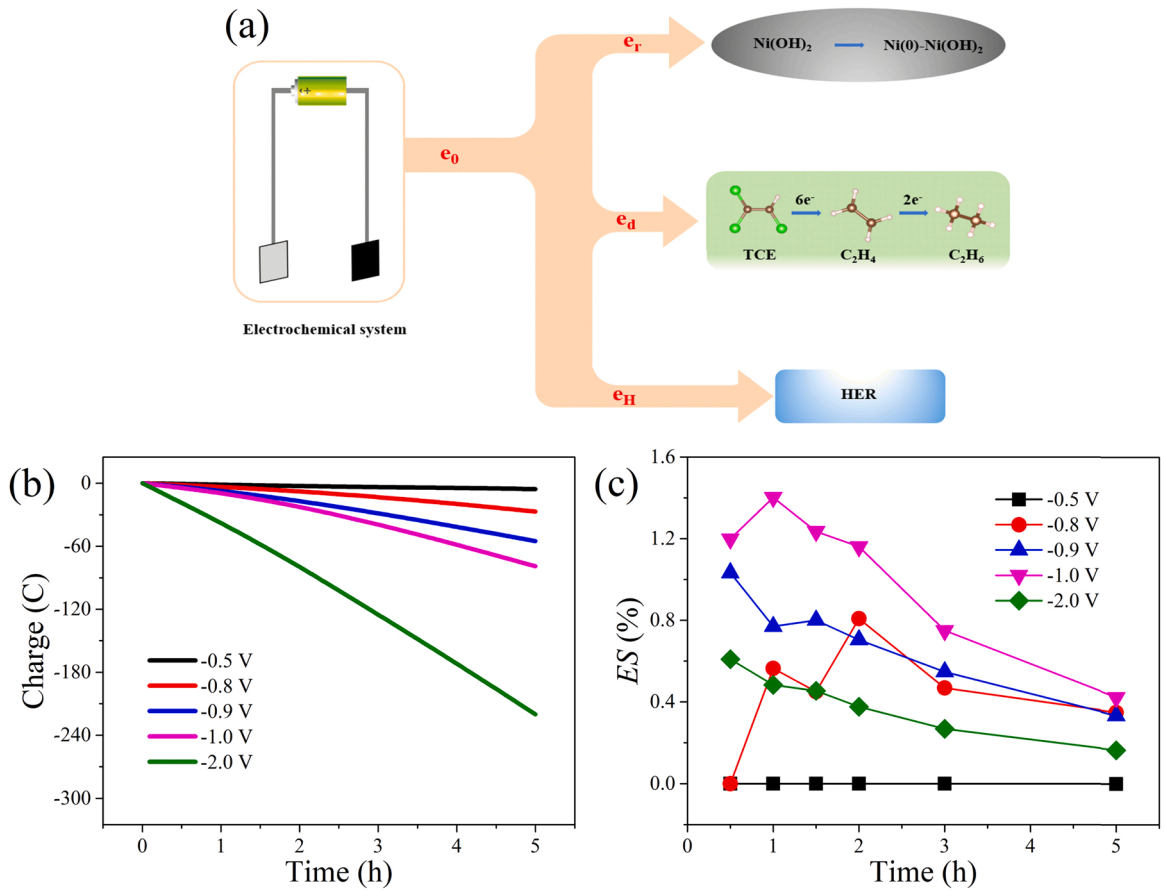

Fig. 4. (a) Schematic illustration of the electron-transfer processes during electrochemical reduction of TCE. (b) Charge input during electrochemical reduction process at different potentials. (c) The electron selectivity efficiency at different potentials. Experimental conditions: electrolyte = 2 mM Na_2SO_4, initial TCE concentration = 25 μM, pH = 7.0.

be adsorbed on the surface of Ni(0)-$Ni(OH)_2$ cathode. For the initial addition of 360 mM methanol, $Ni(OH)_2$ cathode can only be self-activated through the first pathway, which results in the formation of less number of Ni(0) sites. In the case of 360 mM methanol added after one hour of electrolysis, sufficient number of Ni(0) sites had been formed in $Ni(OH)_2$. Even if H* was completely quenched after one hour, TCE can still obtain electrons through Ni(0) sites. Therefore, Fig. 5f showed the high selectivity of formed Ni(0)-$Ni(OH)_2$ towards TCE dechlorination in the presence of high concentration of methanol.

The whole electrochemical process was simulated via DFT analysis. The conformation of $Ni(OH)_2$ was optimized (Fig. S24). The theoretical spin-state of $Ni(OH)_2$ is singlet. When two electrons attach to $Ni(OH)_2$, the atomic charge of Ni decreases from 1.045 to –0.079 and the bond length of Ni–O increases from 1.763 Å to 1.967 Å. After the attachment of two electrons onto the OH groups in $Ni(OH)_2$, two OH^- dissociate from Ni atoms causing the formation of Ni(0). The calculated reduction potential ($E^{0,}$) of $Ni(OH)_2$ is −1.2 V according to Eq. 10:

$$E^{0,} = (G - G')/(nF) - SHE \quad (10)$$

where G and G′ represent the Gibbs free energy of $Ni(OH)_2$ and Ni $(OH)_2 + 2e^-$ conformations, respectively; n represents the number of electrons attached; F is Faraday constant (96,485.34 C/mol); SHE is the standard hydrogen electrode potential (4.44 V).

The $E^{0,}$ of $Ni(OH)_2$ (–1.2 V) is relatively close to the experimental value (ranging from –0.8 to −0.9 V). After $Ni(OH)_2$ accepts two electrons, H^+ combines with the anionic conformation of $Ni(OH)_2$ to form Ni $(OH)_2$-2 H* complexes (Fig. S25). Similarly, $Ni(OH)_2$-2 H* can also be formed by H* attack. The analysis shows that the generation of Ni(0) is thermodynamically favorable once the electrons are transferred (Fig. S26).

Ni(0) cluster is generated from the reduction of $Ni(OH)_2$ at −1.0 V, which plays an important role in TCE hydrodechlorination. Thus, we optimized the geometries of tetratomic Ni cluster (Ni_4) with various spin states according to a previous study (Fig. S27) [67]. The energy of Ni_4 with different spin states is shown in Fig. S28. The optimized results show the quintet spin conformation of Ni_4 with the lowest energy is the ground state, which is in line with findings of a previous publication [67]. Subsequently, the geometries and spin density of Ni_4 cluster-TCE complex were optimized (Fig. S29) [68]. The adsorption of TCE onto Ni_4 cluster leads to the dissociation of the π bond and the formation of two C−Ni σ bonds. The binding energy between TCE and Ni_4 is −20.04 kcal/mol, indicating the adsorption of TCE by Ni_4 is thermodynamically favorable. The theoretical calculation result is supported by the experimental result shown in Fig. 3b-c. At the potential of –0.8 and −0.9 V, the presence of a small amount of Ni(0) causes the reduction of TCE at a relatively slow rate. Thus, a fraction of the TCE molecules remains adsorbed on Ni(0) sites rather than being reduced followed by the release as dechlorination products. Therefore, the carbon balance and chlorine balance curves decreased when the potentials were –0.8 and −0.9 V. As shown in Fig. S30, the binding energy between methanol and Ni_4 is 38.07 kcal/mol. Thus, TCE molecules in solution tend to transfer to Ni(0) sites in the presence of methanol (Fig. 5f). Notably, the energy barrier for the reaction between H* and methanol is only 8.09 kcal mol^{-1} (Fig. S31), which was lower than the binding energy between methanol molecule and Ni_4 cluster (38.07 kcal mol^{-1}). Thus, H* prefers to leave the surface of Ni(0) to react with methanol in bulk solution, leading to the formation of H_2.

The dechlorination of TCE resulted from direct electron transfer and

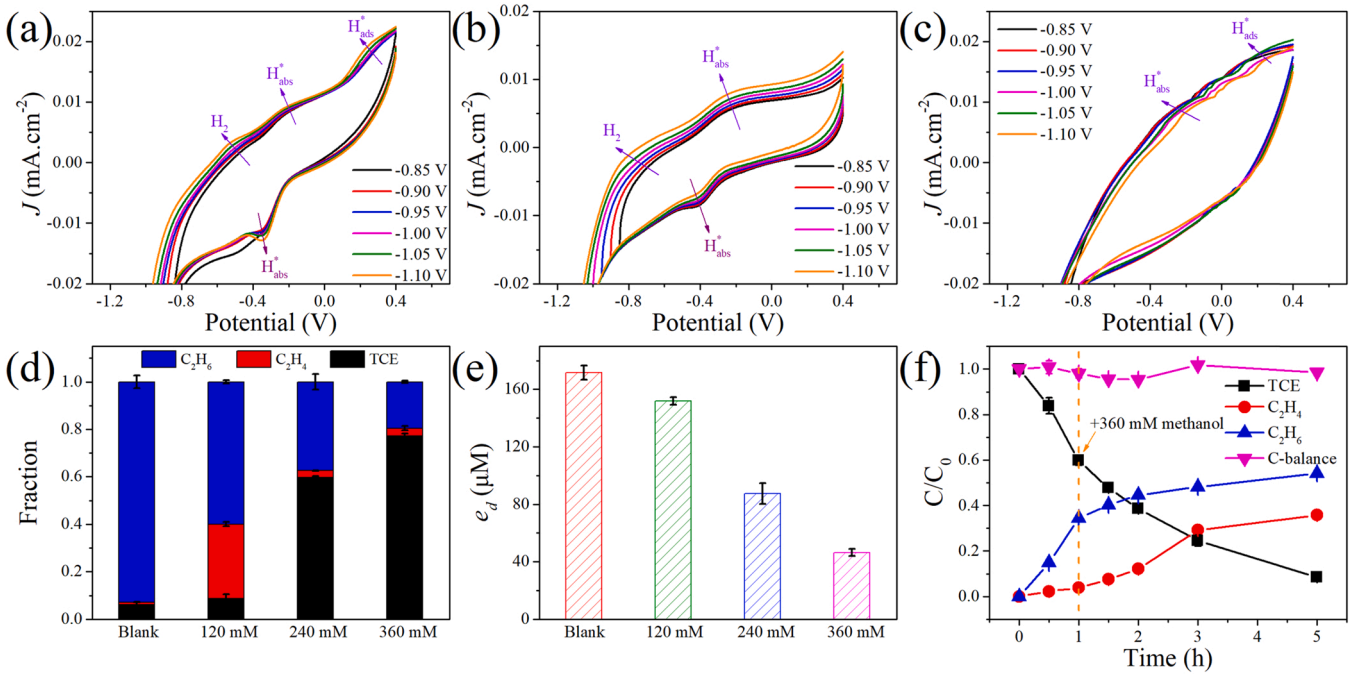

Fig. 5. CVs of Ni(0)-Ni$(OH)_2$ cathode (a) in the absence of TCE, in the presence of (b) 0.4 mM TCE and (c) 120 mM methanol. The cathodic scan with a rate of 50 mV/s started from 0.4 V vs. Ag/AgCl. Experimental conditions: pH = 7.0, electrolyte = 50 mM Na_2SO_4. (d) Product distribution after five hours of electrolysis in the presence of methanol with different concentrations. (e) The calculated e_d value in the presence of methanol with different concentrations. (f) TCE hydrodechlorination by Ni$(OH)_2$ electrode when 360 mM methanol was added after one hour of electrolysis. Experimental conditions: electrolyte = 2 mM Na_2SO_4, applied potential = –1.0 V, initial TCE concentration = 25 μM.

H* attack. For the Ni_4-TCE complex, electrons can be directly transferred from Ni_4 to TCE. The LUMO was distributed on the Cl atom in Ni_4-TCE complex (Fig. S29). Thus, Ni_4-TCE may be dechlorinated to Ni_4-DCE after accepting electrons. Then, Ni_4-DCE is dechlorinated to Ni_4-VC and Ni_4-C_2H_4 after accepting electrons. The charge transfer from Ni_4 cluster to pollutants for Ni_4-TCE, Ni_4-DCE and Ni_4-VC complexes conformations were 0.868, 0.803 and 0.592, respectively (Fig. 6a). This result indicates the Ni_4-pollutant complexes conformations were favorable for electron transfer. The whole dechlorination process via direct electron is shown in Fig. 6b, and the highest free energy barrier is 0.53 eV (Fig. 6c).

For H* attack, H^+ was catalyzed to form H* on Ni_4 cluster where TCE hydrodechlorination occurs [69]. Thus, H^+ was catalyzed by Ni_4 to form Ni_4-2 H first which adsorbs TCE to form Ni_4-2 H-TCE. Then H* species attack the Cl−C bonds in Ni_4-2 H-TCE after dissociative adsorption, leading to a partial or complete dechlorination to form Ni_4-2 H-VC and Ni_4-C_2H_4 with the release of HCl [20]. Finally, H* species attack the π bond of C_2H_4 to form C_2H_6. According to calculated results, H* attack C_2H_4 to form C_2H_6 which releases 514.18 kJ/mol energy. On the other hand, H* reacts with Ni$(OH)_2$ to form Ni(0) releasing 228.16 kJ/mol energy. From the perspective of thermodynamics, the hydrogenation of C_2H_4 is favorable in the presence of H* . The positive and negative phase of the HOMO in the Cl site matches with the H* site in Ni_4-2 H-TCE and Ni_4-2 H-VC complex, demonstrating H* on Ni_4 prefers to attack Cl-C bonds (Fig. S32). The proposed hydrodechlorination process involving H* attack is shown in Fig. 6d. As shown in Fig. 6e, the highest free energy barrier was found to be 1.23 eV for H* formation on the Ni_4 cluster. The free energy barrier of TCE hydrodechlorination was found to be only 0.06 eV, demonstrating that H* formed on Ni(0) is more reactive than direct electron transfer from Ni(0) towards TCE hydrodechlorination.

The schematic diagram about the mechanism of Ni$(OH)_2$ cathode self-activation and the proposed pathways of TCE dechlorination on Ni (0)-Ni$(OH)_2$ cathode was shown in Fig. 7. In summary, a small fraction of Ni(II) sites in Ni$(OH)_2$ on cathode was firstly reduced to Ni(0) electrochemically. Also, the as-formed Ni(0) active sites may catalyze H^+/H_2O to generate H* , thereby accelerating the further generation of Ni (0). Meanwhile, the formed Ni(0) can bind TCE thermodynamically. The hydrodechlorination of TCE occurs on Ni(0)-Ni$(OH)_2$ via direct electron transfer and H* attack. When TCE was transformed to C_2H_6, the C_2H_6 molecule was released from the surface of Ni(0)-Ni$(OH)_2$ cathode. The adsorption of TCE and chlorine-containing intermediates on Ni(0)-Ni $(OH)_2$ electrodes is the cause of carbon imbalance during electrolysis at −0.8 V and −0.9 V. When the potential was more negative than −1.0 V, the strong hydrogenolysis leads to the occurrence of β-elimination after the breakage of one C–Cl bond. In the possible application of the proposed technique, the applied potential should be more negative than −1.0 V to avoid the possible formation of toxic DCEs.

3.5. *Effect of pH*

The effect of pH on TCE-to-ethane conversion was investigated. The hydrodechlorination efficiency of TCE were 100.0%, 94.7%, 82.4% and 84.7% at pH 3.0, 5.0, 9.0 and 11.0, respectively (Fig. S33a–d). The self-activated Ni$(OH)_2$ cathode maintained a strong reductive activity under both acidic and alkaline conditions. Obviously, the hydrodechlorination efficiency of TCE by self-activated Ni$(OH)_2$ cathode under acidic conditions was higher than that under neutral and alkaline conditions. The current density increased more rapidly at low pH values along electrolysis (Fig. 8a), indicating that acidic conditions favored the self-activation of the Ni$(OH)_2$ cathode. The Ni(0)-Ni$(OH)_2$ cathode formed under acidic conditions had higher HER activity than that formed under neutral and alkaline conditions (Fig. 8b), demonstrating the presence of H^+ favors the reduction of Ni(II) to Ni(0). Thus, the LSV of Ni$(OH)_2$ suspension was carried out at different pH conditions to investigate the effect of pH on the reduction of Ni(II) to Ni(0). The potential of Ni(II) reduction peak was not changed in the pH range from 5.0 to 9.0 (Fig. 8c), indicating the reduction potential of Ni(II) in Ni$(OH)_2$ was not affected in this range. In addition, the cathodic current for pH 5.0 at −1.0 V was higher than that for pH 7.0 and pH 9.0. Apart from the high HER under acidic conditions, the dominant H^+ may also enhanced the dehydroxylation of Ni$(OH)_2$ on cathode accelerating the formation of Ni

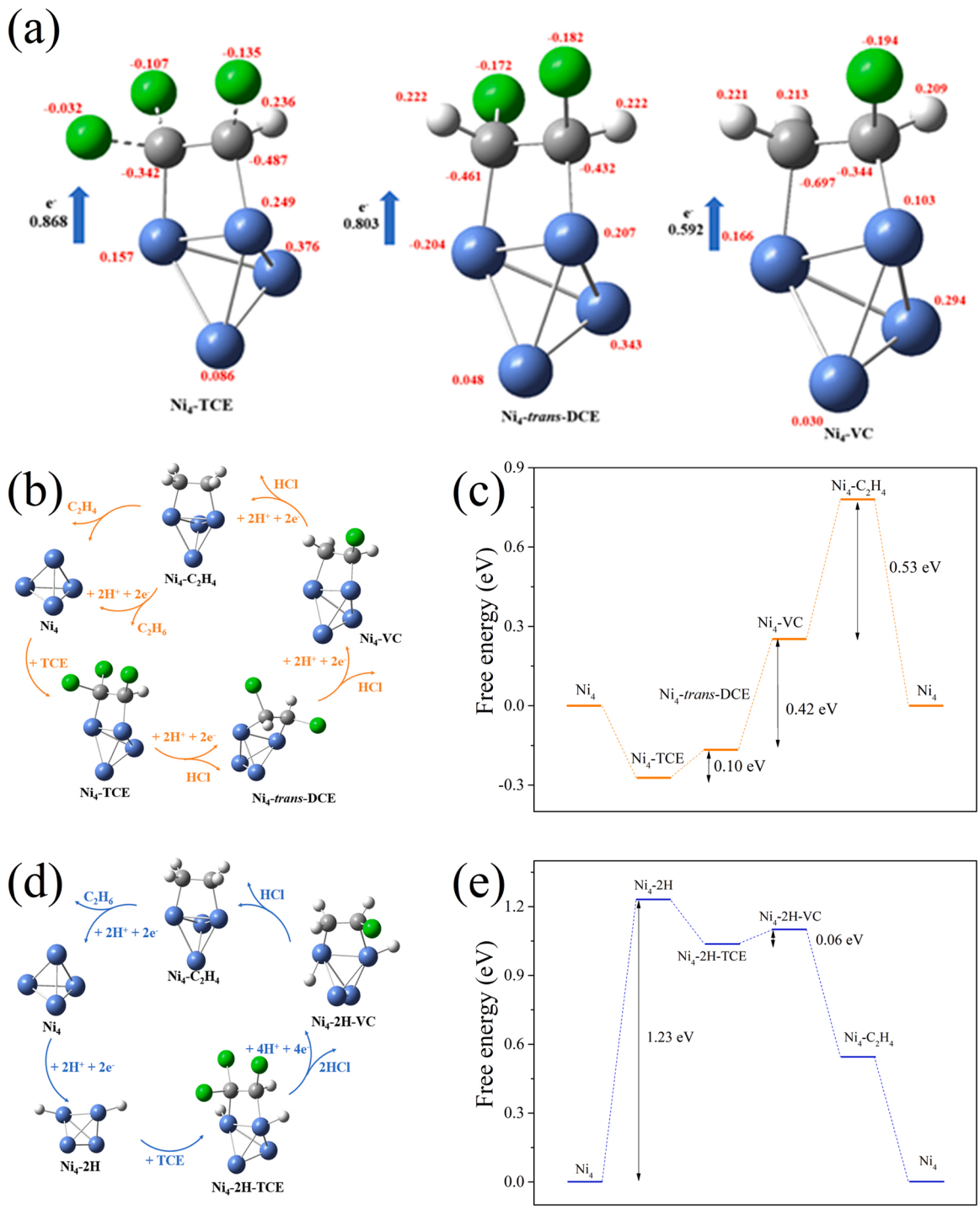

Fig. 6. (a) The conformations of $Ni(OH)_2$-TCE, $Ni(OH)_2$-*trans*-DCE and $Ni(OH)_2$-VC complexes. Numbers with red fonts represent atomic charge. (b) Illustration of the TCE dechlorination pathway on Ni_4 via direct electron transfer and (c) the corresponding Gibbs free energy diagram. (d) Illustration of the H* -mediated TCE dechlorination pathway on Ni_4 and (e) the corresponding Gibbs free energy diagram.

(0) sites. The formed Ni(0) active sites catalyze H^+ to generate H* , thereby further accelerating the generation of Ni(0). The reduction peak of Ni(II) was not obvious at pH 11.0 indicating the dominant OH^- inhibited the dehydroxylation of $Ni(OH)_2$ under alkaline conditions which slowed down the formation rate of Ni(0) sites. The LSV of $Ni(OH)_2$ suspensions at pH 3.0 did not show the reduction peak of Ni(II). The structure of $Ni(OH)_2$ was easily deconstructed and released free Ni^{2+} at pH 3.0. Thus, the concentration of free Ni^{2+} in the electrolyte after 5 h of electrolysis using the $Ni(OH)_2$ cathode under acidic condition was higher than that under neutral and alkaline conditions (Fig. S34). HER consumes relative more electrons compared with hydrodechlorination at low pH values, which resulted in the inconsistency between the TCE-to-ethane conversion and the electron selectivity efficiency (*ES* values). As shown in Fig. 8d, The *EC* values for 5 h electrolysis in the 30 mL reaction system at pH 3, 5, 7, 9 and 11 were 2.43, 1.07, 2.15, 1.94 and 0.93 kWh log^{-1} m^{-3}, respectively. In general, $Ni(OH)_2$ cathode showed high reactivity for the reduction of TCE to C_2H_6 at a very wide pH range from 3 to 11, which demonstrates the applicability of $Ni(OH)_2$ cathode in practical applications.

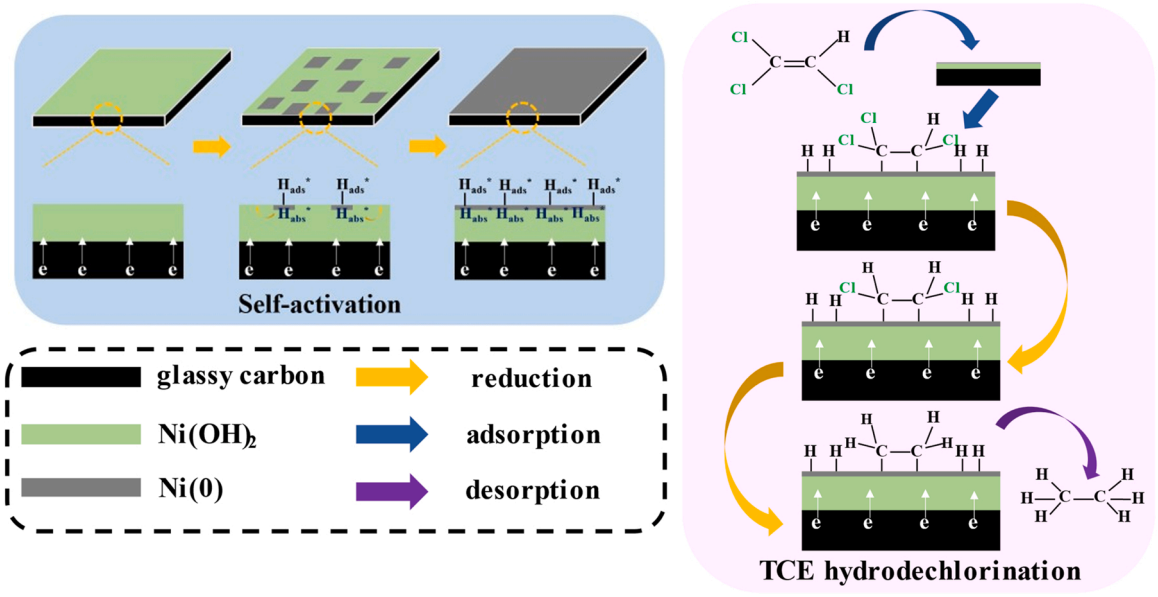

Fig. 7. Schematic diagram of the proposed mechanism of $Ni(OH)_2$ cathode self-activation and the proposed pathways of TCE dechlorination on Ni(0)-$Ni(OH)_2$ cathode.

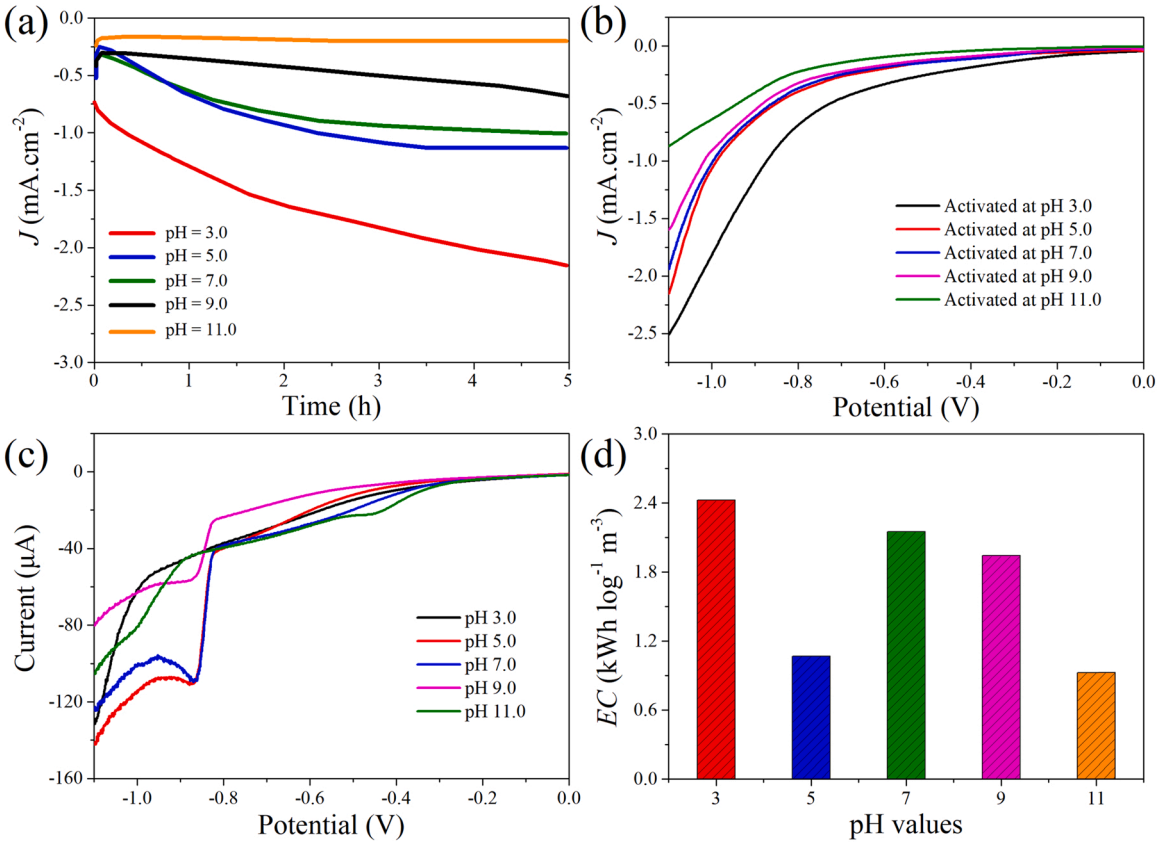

Fig. 8. (a) The change of current density during the electrolysis under different pH conditions. (b) LSV of self-activated $Ni(OH)_2$ cathode after 5 h of electrolysis at different pH values, the pH of the LSV experiment is 7.0. (c) LSV of $Ni(OH)_2$ suspension in 50 mM Na_2SO_4 aqueous solution at different pH values. (d) The normalized energy consumptions (*EC*) of the electrochemical dechlorination process at different pH values.

3.6. Application of self-activated $Ni(OH)_2$ electrode

In real groundwater, the Ca^{2+}, Mg^{2+}, Fe^{2+} and humic acid are widespread [70]. Thus, the effect of Ca^{2+}, Mg^{2+}, Fe^{2+} and humic acid on the performance of self-activated $Ni(OH)_2$ system were investigated. The removal efficiency of TCE was decreased slightly in the presence of Ca^{2+}, Mg^{2+} and humic acid (Fig. 9a). However, the transformation of TCE to C_2H_6 was significantly inhibited in the presence of the studied metal ions and humic acid (Fig. 9b). Ca^{2+} and Mg^{2+} could be immobilized at the surface of electrocatalyst and enhance their binding energy towards

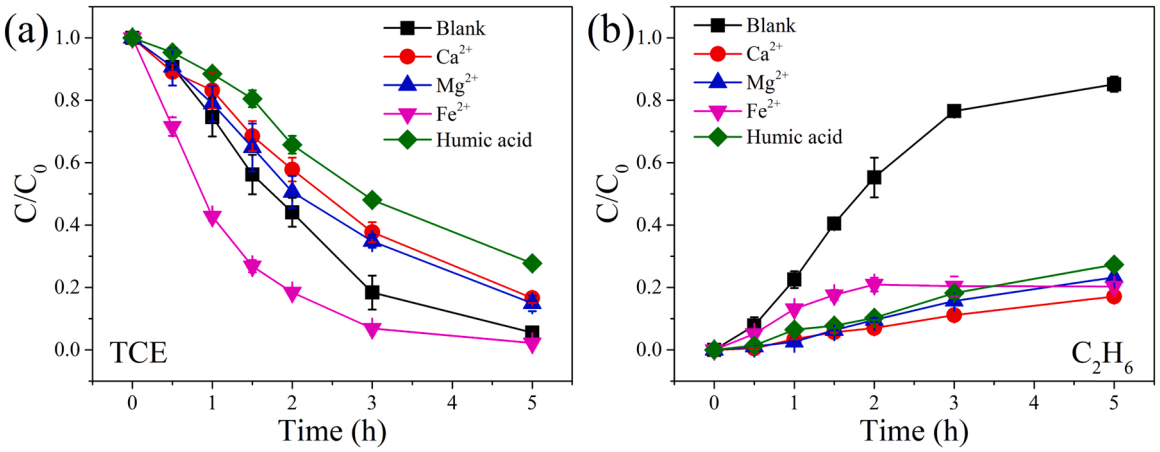

Fig. 9. (a) TCE removal and (b) C_2H_6 generation during the electrolysis in the presence of Ca^{2+} (40 mg/L), Mg^{2+} (10 mg/L), Fe^{2+} (10 mg/L) and humic acid (10 mg/L). Experimental conditions: electrolyte = 2 mM Na_2SO_4, initial TCE concentration = 25 μM, pH = 7.0.

C═C bond due to the polarization effects and the weak donor-acceptor orbital interactions [71]. Therefore, Ca^{2+} and Mg^{2+} immobilized on the surface of $Ni(OH)_2$ frameworks may affect the sorption of TCE. Humic acid may act as an electron acceptor in the system to consume the electrons used for TCE reduction [16]. The presence of Fe^{2+} accelerate the removal of TCE but also inhibited the generation of dechlorination products. The added Fe^{2+} could be oxidized to $Fe(OH)_3$ by dissolved oxygen under neutral conditions. Ferrous and ferric hydroxides may precipitate TCE in solution without dechlorination [72]. Thus, the removal of TCE from solution was enhanced, but the generation of dechlorination products was inhibited.

The $Ni(OH)_2$ electrode was reused five times to evaluate its stability and reusability. The first four runs all showed more than 82.2% of TCE removal efficiency after five hours of electrolysis (Fig. S35), and TCE was completely transformed to C_2H_6 (Fig. 10a–c). The TCE reduction rates in second and third runs were higher than that of the first run because the Ni(0) active sites have been formed in the first run. The formation of Ni(0) in the first run resulted in the generation of H* species at the start of the second and third runs. TCE adsorption occurs on the surface of self-activated $Ni(OH)_2$ cathode and the reaction follows Langmuir-Hinshelwood kinetics (Text S6, Fig. S36) [73,74]. The calculated surface area-normalized pseudo-first-order initial rate constants (r_0) of the second to fifth runs were 2.08, 2.00, 1.62 and 0.87 h^{-1}, respectively (Fig. S37). In the first run, the number of Ni(0) active sites

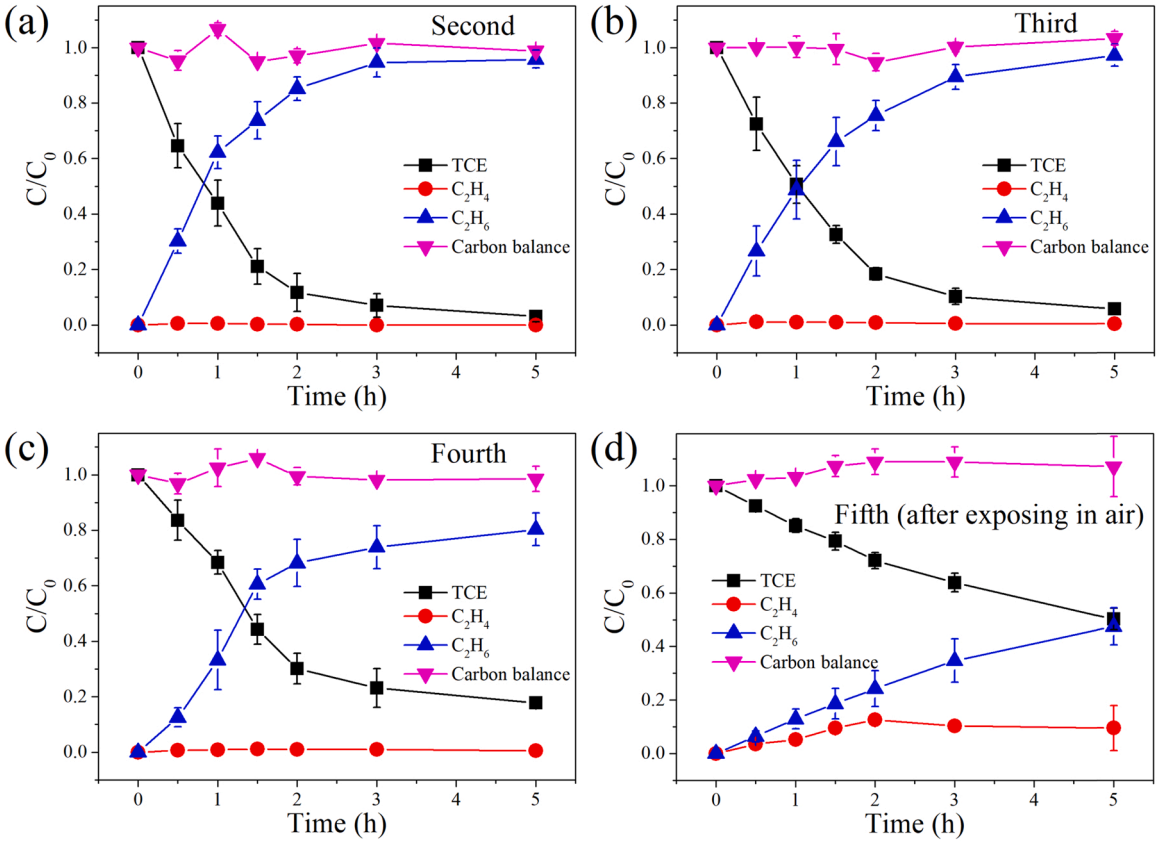

Fig. 10. TCE hydrodechlorination in the (a) second, (b) third, (c) fourth run, and (d) fifth run where the Ni(0)-$Ni(OH)_2$ electrode was exposed in air for 24 h prior the electrolysis. Experimental conditions: electrolyte = 2 mM Na_2SO_4, applied potential = –1.0 V, initial TCE concentration = 25 μM.

increased continuously during $Ni(OH)_2$ self-activation. Thus, r_0 value of the first run is inaccurate. Notably, the r_0 values gradually decreased after the second reuse cycle. This result may be attributed to the slow deactivation of Ni(0) active sites after their reaction with TCE. After the fourth run, the Ni(0)-$Ni(OH)_2$ cathode was exposed in air for 24 h followed by one more run for TCE removal. The TCE removal efficiency decreased from 82.2% to 49.8% because a fraction of the generated Ni (0) catalytic sites was oxidized in air. The conversion of C_2H_4 to C_2H_6 was also inhibited (Fig. 10d), demonstrating a decreased amount of generated H* once the Ni(0) active sites were oxidized. It is speculated that only part of the air-oxidized Ni(0) sites could be reduced electrochemically to their original state, which led to a decreased removal efficiency of TCE and an inhibited conversion of C_2H_4 to C_2H_6. In contrast, Ni cathode showed no reactivity towards TCE dechlorination after exposure in air for 24 h (Fig. S3c). Once pristine Ni electrode is exposed in air, the metal oxide layer quickly envelops the whole Ni electrode. However, parts of the air-oxidized Ni(0) could be reactivated electrochemically, maintaining a relatively high reactivity for TCE hydrodechlorination. The concentration of released Ni^{2+} in consecutive runs is shown in Fig. S38. A small amount of free Ni^{2+} (71 μM) was released into the electrolyte during the first run using the freshly prepared Ni $(OH)_2$ electrode. However, once the Ni(0)-$Ni(OH)_2$ structure was formed, the release of free Ni^{2+} during electrolysis was significantly inhibited. In order to avoid the secondary pollution caused by the released Ni, the Ni-contaminated electrolyte of the first 5 h electrolysis for $Ni(OH)_2$ cathode self-activation should be carefully treated. Then, the formed Ni(0)-$Ni(OH)_2$ cathode after self-activation is recommended for further consideration and testing as a potential technology for the remediation of real groundwater because of the extremely low Ni dissolution.

In order to investigate whether TCE can be dechlorinated in the presence of $Ni(OH)_2$ in solution, we used glassy carbon electrode as working electrode and added 5 mM of $Ni(OH)_2$ into the electrolyte for TCE dechlorination. As shown in Fig. S39a, 67.9% TCE was reduced to C_2H_6 after 5 h of electrolysis. However, Ni(0) was not observed in the suspension particles after electrolysis (Fig. S39b). Since $Ni(OH)_2$ particles cannot dechlorinate TCE (Fig. S5a), $Ni(OH)_2$ particles could be reduced and precipitate as Ni(0)-$Ni(OH)_2$ on the cathode surface which is reactive for TCE dechlorination. Although TCE can be dechlorinated in the presence of $Ni(OH)_2$ particles in the solution, the dosage of $Ni(OH)_2$ was much higher compared with the self-activated $Ni(OH)_2$ cathode. Also, the separation of added $Ni(OH)_2$ particles from the treated water is problematic in future practical applications. Thus, we believe the deposition of $Ni(OH)_2$ catalyst on the electrode surface is a more feasible and effective approach than addition of $Ni(OH)_2$ into treated water as particles.

4. Conclusions

In this work, Ni(0)-$Ni(OH)_2$ electrode was self-activated by reduction of $Ni(OH)_2$ for electrochemical hydrodechlorination of TCE to ethane in groundwater. Ni(0) site can be formed after applying a potential more negative than −0.8 V on $Ni(OH)_2$ electrode. The presence of Ni(0) site on Ni(0)-$Ni(OH)_2$ enhanced the adsorption of TCE and subsequent electron transfer process. The active H* generated on the Ni(0) site is highly reactive for the reduction of Ni(II) and hydrodechlorination of TCE to ethane. TCE was completely transformed to ethane after 5 h of electrolysis at −1.0 V. When the potential was more negative than −1.0 V, the intensive HER decreased the electron selectivity towards hydrodechlorination. Direct electron transfer and H* -mediated indirect dechlorination at the generated Ni(0) sites both contributed to the hydrodechlorination of TCE. TCE can be efficiently reduced in low-conductivity groundwater and at a very wide pH range, from pH 3 to pH 11. The TCE-to-ethane conversion efficiency was higher than 82.2% during four consecutive runs using the same $Ni(OH)_2$ electrode. Although the self-activating $Ni(OH)_2$ cathode shows extremely strong hydrodechlorination activity towards TCE, the antioxidant capacity and metal dissolution control capacity of Ni(0)-$Ni(OH)_2$ still need to be further enhanced. This work shows the low cost, stable, and easy-to-prepare $Ni(OH)_2$ is a promising highly active electrocatalyst that can be further considered as a potential suitable replacement of precious metals in applications focused on the electrochemical reduction of COCs.

CRediT authorship contribution statement

Jia Deng: Validation, Investigation, Writing – original draft. **Feng Wu:** Supervision, Writing – review & editing. **Shuxian Gao:** Formal analysis. **Dionysios D. Dionysiou:** Writing – review & editing. **Li-Zhi Huang:** Conceptualization, Methodology, Project administration, Funding acquisition, Writing – review & editing, Investigation.

Declaration of Competing Interest

The authors declare that they have no known competing financial interests or personal relationships that could have appeared to influence the work reported in this paper.

Acknowledgements

The current work was financially supported by the National Natural Science Foundation of China (Grant No. 41807188 and 51978537), the Fundamental Research Funds for the Central Universities (2042021kf0201), and Start-up Fund for Distinguished Scholars, Wuhan University (1403-413100041, 1403-600460022). The numerical calculations in this paper have been done on the supercomputing system in the Supercomputing Center of University of Science and Technology of China.

Appendix A. Supporting information

Supplementary data associated with this article can be found in the online version at doi:10.1016/j.apcatb.2022.121258.

References

[1] Y. Wu, Z. Jiang, Z. Lin, Y. Liang, H. Wang, Direct electrosynthesis of methylamine from carbon dioxide and nitrate, Nat. Sustain. 4 (2021) 725–730.
[2] S. Gushgaridoyle, L. Alvarezcohen, Effects of arsenic on trichloroethene–dechlorination activities of dehalococcoides mccartyi 195, Environ. Sci. Technol. 54 (2020) 1276–1285.
[3] J.A. Hopple, G.C. Delzer, J.A. Kingsbury, Anthropogenic Organic Compounds in Source Water of Selected Community Water Systems that Use Groundwater, 2002–05, 2009.
[4] A. Gafni, H. Siebner, A. Bernstein, Potential for co-metabolic oxidation of TCE and evidence for its occurrence in a large-scale aquifer survey, Water Res. 171 (2020), 115431.
[5] H. Yin, X. Cao, C. Lei, W. Chen, B. Huang, Insights into electroreductive dehalogenation mechanisms of chlorinated environmental pollutants, ChemElectroChem 7 (2020) 1825–1837.
[6] C. Lei, F. Liang, J. Li, W. Chen, B. Huang, Electrochemical reductive dechlorination of chlorinated volatile organic compounds (Cl-VOCs): effects of molecular structure on the dehalogenation reactivity and mechanisms, Chem. Eng. J. 358 (2019) 1054–1064.
[7] X. Mao, A. Ciblak, K. Baek, M. Amm, R. Loch-Caruso, A.N. Alshawabkeh, Optimization of electrochemical dechlorination of trichloroethylene in reducing electrolytes, Water Res. 46 (2012) 1847–1857.
[8] Q. Wen, T. Yang, S. Wang, C. Ye, L. Cong, Y. Qu, Dechlorination of 4-chlorophenol to phenol in bioelectrochemical systems, J. Hazard. Mater. 244–245 (2013) 743–749.
[9] J.I. Han, S. Lontoh, J.D. Semrau, Degradation of chlorinated and brominated hydrocarbons by Methylomicrobium album BG8, Arch. Microbiol. 172 (1999) 393–400.
[10] X. Maymógatell, I. Nijenhuis, S.H. Zinder, Reductive dechlorination of cis-1,2-dichloroethene and vinyl chloride by "Dehalococcoides ethenogenes", Environ. Sci. Technol. 35 (2001) 516–521.
[11] O. Lugaresi, J.V. Perales-Rondon, A. Minguzzi, J. Solla-Gullon, S. Rondinini, J. M. Feliu, C.M. Sanchez-Sanchez, Rapid screening of silver nanoparticles for the catalytic degradation of chlorinated pollutants in water, Appl. Catal. B Environ. 163 (2015) 554–563.

[12] B.M. Hryniewicz, L. Bach-Toledo, M. Vidotti, Harnessing energy from micropollutants electrocatalysis in a high-performance supercapacitor based on PEDOT nanotubes, Appl. Mater. Today 18 (2020), 100538.

[13] A.A. Arpia, W.H. Chen, S.L. Su, P. Rousset, M. Luna, Sustainable biofuel and bioenergy production from biomass waste residues using microwave-assisted heating: A comprehensive review, Chem. Eng. J. 403 (2021), 126233.

[14] I.M.S.K. Ilankoon, Y. Ghorbani, N.C. Meng, G. Herath, T. Moyo, J. Petersen, E-waste in the international context - A review of trade flows, regulations, hazards, waste management strategies and technologies for value recovery, Waste Manag. 82 (2018) 258–275.

[15] Trichloroethylene, in: WHO (Ed.), WHO Regional Office for Europe, Copenhagen, Denmark, 2000.

[16] B. Liu, H. Zhang, Q. Lu, G. Li, F. Zhang, A CuNi bimetallic cathode with nanostructured copper array for enhanced hydrodechlorination of trichloroethylene (TCE), Sci. Total. Environ. 635 (2018) 1417–1425.

[17] R. Mao, C. Huang, X. Zhao, M. Ma, J. Qu, Dechlorination of triclosan by enhanced atomic hydrogen-mediated electrochemical reduction: kinetics, mechanism, and toxicity assessment, Appl. Catal. B Environ. 241 (2019) 120–129.

[18] J. Zhang, Q. Ji, H. Lan, G. Zhang, H. Liu, J. Qu, Synchronous reduction–oxidation process for efficient removal of trichloroacetic acid: H* initiates dechlorination and·OH is responsible for removal efficiency, Environ. Sci. Technol. 53 (2019) 14586–14594.

[19] S. Yuan, X. Mao, A.N. Alshawabkeh, Efficient degradation of TCE in groundwater using Pd and electro-generated H_2 and O_2: a shift in pathway from hydrodechlorination to oxidation in the presence of ferrous ions, Environ. Sci. Technol. 46 (2012) 3398–3405.

[20] Y. Luo, C. Zhou, Y. Bi, X. Long, B.E. Rittmann, Long-term continuous Co-reduction of 1,1,1-trichloroethane and trichloroethene over palladium nanoparticles spontaneously deposited on H_2-transfer membranes, Environ. Sci. Technol. 55 (2021) 2057–2066.

[21] W. Guo, J.H. Zou, B.B. Guo, J.H. Xiong, C. Liu, Z.H. Xie, L. Wu, Pd nanoclusters/TiO_2(B) nanosheets with surface defects toward rapid photocatalytic dehalogenation of polyhalogenated biphenyls under visible light, Appl. Catal. B Environ. 277 (2020), 119255.

[22] S.J. Li, Y.L. Fang, C.D. Romanczuk, Z.H. Jin, T.L. Li, M.S. Wong, Establishing the trichloroethene dechlorination rates of palladium-based catalysts and iron-based reductants, Appl. Catal. B Environ. 125 (2012) 95–102.

[23] G. Jiang, M. Lan, Z. Zhang, X. Lv, Z. Lou, X. Xu, F. Dong, S. Zhang, Identification of active hydrogen species on palladium nanoparticles for an enhanced electrocatalytic hydrodechlorination of 2,4-dichlorophenol in water, Environ. Sci. Technol. 51 (2017) 7599–7605.

[24] Y.L. Han, C.J. Liu, J. Horita, W.L. Yan, Trichloroethene hydrodechlorination by Pd-Fe bimetallic nanoparticles: Solute-induced catalyst deactivation analyzed by carbon isotope fractionation, Appl. Catal. B Environ. 188 (2016) 77–86.

[25] P. Dabo, A. Cyr, F. Laplante, F. Jean, H. Ménard, J. Lessard, Electrocatalytic dehydrochlorination of pentachlorophenol to phenol or cyclohexanol, Environ. Sci. Technol. 34 (2000) 1265–1268.

[26] J. Li, H. Wang, Z. Qi, C. Ma, Z. Zhang, B. Zhao, L. Wang, H. Zhang, Y. Chong, X. Chen, X. Cheng, D.D. Dionysiou, Kinetics and mechanisms of electrocatalytic hydrodechlorination of diclofenac on Pd-Ni/PPy-rGO/Ni electrodes, Appl. Catal. B Environ. 268 (2020), 118696.

[27] K. Wiltschka, L. Neumann, M. Werheid, M. Bunge, R.A. During, K. Mackenzie, L. Bohm, Hydrodechlorination of hexachlorobenzene in a miniaturized nano-Pd(0) reaction system combined with the simultaneous extraction of all dechlorination products, Appl. Catal. B Environ. 275 (2020), 119100.

[28] B.J. Shields, B. Kudisch, G.D. Scholes, A.G. Doyle, Long-lived charge transfer states of nickel(II) aryl halide complexes facilitate bimolecular photoinduced electron transfer, J. Am. Chem. Soc. 140 (2018) 3035–3039.

[29] Z. Mao, P.G. Lustemberg, J.R. Rumptz, M.V. Ganduglia-Pirovano, C.T. Campbell, Ni nanoparticles on CeO_2(111): Energetics, electron transfer and structure by Ni adsorption calorimetry, spectroscopies and DFT, ACS Catal. 10 (2020) 5101–5114.

[30] F. He, Z. Li, S. Shi, W. Xu, H. Sheng, Y. Gu, Y. Jiang, B. Xi, Dechlorination of excess trichloroethene by bimetallic and sulfidated nanoscale zero-valent iron, Environ. Sci. Technol. 52 (2018) 8627–8637.

[31] G.K. Parshetti, R.A. Doong, Dechlorination of chlorinated hydrocarbons by bimetallic Ni/Fe immobilized on polyethylene glycol-grafted microfiltration membranes under anoxic conditions, Chemosphere 86 (2012) 392–399.

[32] R.S. Sahu, R.A. Doong, Functionalized Fe/Ni@g-C3N4 nanostructures for the enhanced trichloroethylene dechlorination and successive oxygen reduction reaction activity, Environ. Sci. Nano (2020).

[33] L.L. Feng, G. Yu, Y. Wu, G.D. Li, L. Hui, Y. Sun, T. Asefa, W. Chen, X. Zou, High-index faceted Ni_3S_2 nanosheet arrays as highly active and ultrastable electrocatalysts for water splitting, J. Am. Chem. Soc. 137 (2015) 14023–14026.

[34] Ledendecker Marc, KrickCalderón Sandra, Papp Christian, Steinrück Hans-Peter, Antonietti Markus, The synthesis of nanostructured Ni_5P_4 films and their use as a non-noble bifunctional electrocatalyst for full water splitting, Angew. Chem. Int. Ed. 127 (2015) 12361–12365.

[35] B.W. Xue, C.H. Zhang, Y.Z. Wang, W.W. Xie, N.W. Li, L. Yu, Recent progress of Ni–Fe layered double hydroxide and beyond towards electrochemical water splitting, Nanoscale Adv. 2 (2020) 5555–5566.

[36] L. Rajic, N. Fallahpour, E. Oguzie, A. Alshawabkeh, Electrochemical transformation of thichloroethylene in groundwater by Ni-containing cathodes, Electrochim. Acta 181 (2015) 118–122.

[37] Y. Han, C. Liu, J. Horita, W. Yan, Trichloroethene (TCE) hydrodechlorination by NiFe nanoparticles Influence of aqueous anions on catalytic pathways, Chemosphere 205 (2018) 404–413.

[38] S. Niu, W.J. Jiang, T. Tang, Y. Zhang, J.H. Li, J.S. Hu, Facile and scalable synthesis of robust $Ni(OH)_2$ nanoplate arrays on NiAl foil as hierarchical active scaffold for highly efficient overall water splitting, Adv. Sci. 4 (2017) 1700084.

[39] J. Hu, S. Li, Y. Li, J. Wang, Y. Du, Z. Li, X. Han, J. Sun, P. Xu, A crystalline–amorphous Ni–$Ni(OH)_2$ core–shell catalyst for the alkaline hydrogen evolution reaction, J. Mater. Chem. A 8 (2020) 23323–23329.

[40] M. Chhetri, S. Sultan, C. Rao, Electrocatalytic hydrogen evolution reaction activity comparable to platinum exhibited by the Ni/$Ni(OH)_2$/graphite electrode, Proc. Natl. Acad. Sci. USA 114 (2017) 8986–8990.

[41] Y. Tang, L. Dong, H.B. Wu, X.Y. Yu, Tungstate-modulated Ni/$Ni(OH)_2$ interface for efficient hydrogen evolution reaction in neutral media, J. Mater. Chem. A 9 (2021) 1456–1462.

[42] R. Subbaraman, D. Tripkovic, D. Strmcnik, K.C. Chang, M. Uchimura, A. P. Paulikas, V. Stamenkovic, N.M. Markovic, Enhancing hydrogen evolution activity in water splitting by tailoring Li^+-$Ni(OH)_2$-Pt interfaces, Science 334 (2011) 1256–1260.

[43] M. Gong, W. Zhou, M.C. Tsai, J. Zhou, M. Guan, M.C. Lin, B. Zhang, Y. Hu, D. Y. Wang, J. Yang, Nanoscale nickel oxide/nickel heterostructures for active hydrogen evolution electrocatalysis, Nat. Commun. 5 (2014) 4695.

[44] J. Ji, L.L. Zhang, H. Ji, L. Yang, R.S. Ruoff, Nanoporous $Ni(OH)_2$ thin film on 3D ultrathin-graphite foam for asymmetric supercapacitor, ACS Nano 7 (2013) 6237–6243.

[45] L. Dai, Z. Chen, L. Li, P. Yin, H. Zhang, Ultrathin Ni(0)-embedded $Ni(OH)_2$ heterostructured nanosheets with enhanced electrochemical overall water splitting, Adv. Mater. 32 (2020) 1906915.

[46] J. Deng, X.-M. Hu, E. Gao, F. Wu, W. Yin, L.-Z. Huang, D.D. Dionysiou, Electrochemical reductive remediation of trichloroethylene contaminated groundwater using biomimetic iron-nitrogen-doped carbon, J. Hazard. Mater. 419 (2021), 126458.

[47] A.D. Becke, Density-functional thermochemistry. III. The role of exact exchange, J. Chem. Phys. 98 (1998) 5648–5652.

[48] D.J. Van Hoomissen, S. Vyas, Early events in the reductive dehalogenation of linear perfluoroalkyl substances, Environ. Sci. Technol. Lett. 6 (2019) 365–371.

[49] M.J. Frisch, G.W. Trucks, H.B. Schlegel, G.E. Scuseria, J.R.C.M. A. Robb, G. Scalmani, V. Barone, G.A. Petersson, H. Nakatsuji, X. Li, M. Caricato, A. Marenich, J. Bloino, B.G. Janesko, R. Gomperts, B. Mennucci, H.P. Hratchian, J.V. Ortiz, A.F. Izmaylov, J.L. Sonnenberg, D. Williams-Young, F. Ding, F. Lipparini, F. Egidi, J. Goings, B. Peng, A. Petrone, T. Henderson, D. Ranasinghe, V.G. Zakrzewski, J. Gao, N. Rega, G. Zheng, W. Liang, M. Hada, M. Ehara, K. Toyota, R. Fukuda, J. Hasegawa, M. Ishida, T. Nakajima, Y. Honda, O. Kitao, H. Nakai, T. Vreven, K. Throssell, J.A. Montgomery, Jr., J.E. Peralta, F. Ogliaro, M. Bearpark, J.J. Heyd, E. Brothers, K.N. Kudin, V.N. Staroverov, T. Keith, R. Kobayashi, J. Normand, K. Raghavachari, A. Rendell, J.C. Burant, S.S. Iyengar, J. Tomasi, M. Cossi, J.M. Millam, M. Klene, C. Adamo, R. Cammi, J.W. Ochterski, R.L. Martin, K. Morokuma, O. Farkas, J.B. Foresman, D.J. Fox, in: GAUSSIAN 09. Gaussian, Inc., Wallingford, CT, 2009.

[50] P. Jeffrey, H. Willard, R. Wadt, Ab initio effective core potentials for molecular calculations. Potentials for the transition metal atoms Sc to Hg, J. Chem. Phys. 82 (1985) 270-270.

[51] T. Chen, J. Ma, Q. Zhang, Z. Xie, Y. Zeng, Degradation of propranolol by UV-activated persulfate oxidation: Reaction kinetics, mechanisms, reactive sites, transformation pathways and Gaussian calculation, Sci. Total. Environ. 690 (2019) 878–890.

[52] A.V. Marenich, C.J. Cramer, D.G. Truhlar, Universal solvation model based on solute electron density and on a continuum model of the solvent defined by the bulk dielectric constant and atomic surface tensions, J. Phys. Chem. B 113 (2009) 6378–6396.

[53] T. Lu, F. Chen, Multiwfn: a multifunctional wavefunction analyzer, J. Comput. Chem. 33 (2012) 580–592.

[54] S.H. Liang, K.F. Chen, C.S. Wu, Y.H. Lin, C.M. Kao, Development of $KMnO_4$-releasing composites for in situ chemical oxidation of TCE-contaminated groundwater, Water Res. 54 (2014) 149–158.

[55] Y. Xu, Z. Yao, Z. Mao, M. Shi, B. Liu, Single-Ni-atom catalyzes aqueous phase electrochemical reductive dechlorination reaction, Appl. Catal. B Environ. 277 (2020), 119057.

[56] A.A.-G. M, A.-C. Texier, L. Lartundo-Rojas, I. Gonzalez, Electrochemical dechlorination of 2-chlorophenol on Pd/Ti, Ni/Ti and Pd-Ni Alloy/Ti electrodes, J. Electrochem. Soc. 162 (2015) 223–230.

[57] S.B. Pillai, B. Joseph, D. Upadhyay, C. Marini, P.K. Jha, Pressure induced hydrogen order–disorder transition in β-$Ni(OH)_2$, J. Phys. Chem. C 125 (2021) 2785–2792.

[58] W. Zheng, L. Zhu, Z. Yan, Z. Lin, Z. Lei, Y. Zhang, H. Xu, Z. Dang, C. Wei, C. Feng, Self-activated Ni cathode for electrocatalytic nitrate reduction to ammonia: From fundamentals to scale-up for treatment of industrial wastewater, Environ. Sci. Technol. (2021).

[59] E. Cossar, M. Houache, Z. Zhang, E.A. Baranova, Comparison of electrochemical active surface area methods for various nickel nanostructures, J. Electroanal. Chem. 870 (2020), 114246.

[60] J. Miao, F.-X. Xiao, H.B. Yang, S.Y. Khoo, J. Chen, Z. Fan, Y.-Y. Hsu, H.M. CHen, H. Zhang, B. Liu, Hierarchical Ni-Mo-S nanosheets on carbon fiber cloth: a flexible electrode for efficient hydrogen generation in neutral electrolyte, Sci. Adv. 1 (2015) 1500259.

[61] Z. Wu, X.L. Huang, Z.L. Wang, J.J. Xu, H.G. Wang, X.B. Zhang, Electrostatic induced stretch growth of homogeneous β-Ni(OH)2 on graphene with enhanced high-rate cycling for supercapacitors, Rep 4 (2014).

[62] J. Ai, W. Yin, H.C.B. Hansen, Fast dechlorination of chlorinated ethylenes by green rust in the presence of bone char, Environ. Sci. Technol. Lett. 6 (2019) 191–196.

[63] C. Durante, A.A. Isse, G. Sandona, A. Gennaro, Electrochemical hydrodehalogenation of polychloromethanes at silver and carbon electrodes, Appl. Catal. B Environ. 88 (2009) 479–489.
[64] Z. Mao, L. Liu, H.B. Yang, Y. Zhang, Z. Yao, H. Wu, Y. Huang, Y. Xu, B. Liu, Atomically dispersed Pd electrocatalyst for efficient aqueous phase dechlorination reaction, Electrochim. Acta 391 (2021), 138886.
[65] J. Deng, E. Gao, F. Wu, Z. You, X. Li, S. Gao, L.-Z. Huang, Generation of atomic hydrogen by Ni-Fe hydroxides: Mechanism and activity for hydrodechlorination of trichloroethylene, Water Res. 207 (2021), 117802.
[66] S. Bastide, C. Zlotea, M. Laurent, M. Latroche, C. Cachet-Vivier, Direct assessment from cyclic voltammetry of size effect on the hydrogen sorption properties of Pd nanoparticle/carbon hybrids, J. Electroanal. Chem. 706 (2013) 33–39.
[67] S. Goel, A.E. Masunov, Density functional theory study of small nickel clusters, J. Mol. Model. 18 (2012) 783–790.
[68] J. Adhikary, D. Meyerstein, V. Marks, M. Meistelman, G. Gershinsky, A. Burg, D. Shamir, H. Kornweitz, Y. Albo, Sol-gel entrapped Au^0 - and Ag^0 - nanoparticles catalyze reductive de-halogenation of halo-organic compounds by BH_4^-, Appl. Catal. B Environ. 239 (2018) 450–462.
[69] Z. Wu, P. Tao, C. Yan, S. Ge, Y. Ju, T. Li, L. Kai, L. Ling, A. Yip, M. Zhang, Synthesis of palladium phosphides for aqueous phase hydrodechlorination: Kinetic study and deactivation resistance, J. Catal. 366 (2018) 80–90.
[70] Y. Liu, T. Phenrat, G.V. Lowry, Effect of TCE concentration and dissolved groundwater solutes on NZVI-promoted TCE dechlorination and H_2 evolution, Environ. Sci. Technol. 41 (2007) 7881–7887.
[71] J.-H. Guo, H. Zhang, M. Gong, X.-L. Cheng, Ca^{2+}- and Mg^{2+}-doped covalent organic frameworks exhibiting high hydrogen and acetylene storage, Struct. Chem. 24 (2013) 691–703.
[72] X. Mao, S. Yuan, N. Fallahpour, A. Ciblak, J. Howard, I. Padilla, R. Loch-Caruso, A. N. Alshawabkeh, Electrochemically induced dual reactive barriers for transformation of TCE and mixture of contaminants in groundwater, Environ. Sci. Technol. 46 (2012) 12003–12011.
[73] W. Lee, B. Batchelor, Abiotic reductive dechlorination of chlorinated ethylenes by iron-bearing soil minerals. 1. pyrite and magnetite, Environ. Sci. Technol. 36 (2002) 5147–5154.
[74] W. Lee, B. Batchelor, Abiotic reductive dechlorination of chlorinated ethylenes by iron-bearing soil minerals. 2. Green rust, Environ. Sci. Technol. 36 (2002) 5348–5354.